15th Australasian Fluid Mechanics Conference
The University of Sydney, Sydney, Australia
13-17 December 2004

Simulating the Deformation of Newtonian and Non-Newtonian Drops through a Micro-Fluidic Contraction

D.J.E. Harvie[1], M.R. Davidson[1] and J.J. Cooper-White[2]

[1]Department of Chemical and Biomolecular Engineering
The University of Melbourne, VIC, 3010 AUSTRALIA

[2]Division of Chemical Engineering
The University of Queensland, QLD, 4072 AUSTRALIA

Abstract

A numerical parametric study of droplet deformation within an axisymmetric micro-fluidic contraction is performed. Both Newtonian and Non-Newtonian shear-thinning fluids are considered for the droplet phase. Droplet deformation is found to be largest when surface tension forces are lowest, and inertial forces highest. The Non-Newtonian droplets behave quite differently to their Newtonian counterparts, primarily because the high strain rates experienced within the contraction result in low internal viscosities. This can allow instabilities to develop on the droplet surface.

Introduction

In the field of two phase micro-fluidics, the simple contraction is a tool that can be used to stretch, shear, break or otherwise deform a droplet. Droplet behaviour within such micro-sized devices differs from that within larger sized systems because surface effects, such as surface tension forces, assume greater importance. Knowledge of droplet behaviour within such contractions would be beneficial to applications such as micro-reactors, where the controlled deformation of droplets to enhance mixing, heat or mass transfer rates is desirable.

There have been few experimental studies concerned with immiscible fluids passing through micro-fluidic contractions. An exception to this is the work of [1] who used a micro-fluidic contraction as a 'flow focusing' device to break a stream of disperse phase fluid into droplets. The deformation of larger, millimetre sized droplets moving through contractions has been studied experimentally by several researchers, including [4]. Numerical investigations of droplets moving through contractions have generally employed the creeping flow approximation, however, [10] used the full Navier-Stokes equations when simulating droplet deformation through millimetre sized contractions. Droplet deformation in general extensional and shear flows has been extensively studied both experimentally and numerically. [3] and [8] give good reviews of this topic.

The purpose of this study is to perform a parametric numerical study of droplet deformation in an axisymmetric contraction, focusing in particular on regimes relevant to micro-fluidic devices. Due to the importance of organic and polymer suspensions in micro-fluidic applications, we consider shear thinning Non-Newtonian fluids for the disperse phase as well as Newtonian fluids.

Problem Description

As shown in figure 1, the problem under consideration consists of a droplet entrained in a continuous liquid phase passing through a $4:1$ axisymmetric contraction. All lengths are non-dimensionalised by the radius of the inlet R, so that the contraction radius is $1/4$, the contraction length is 5 and the initial droplet diameter is 1.

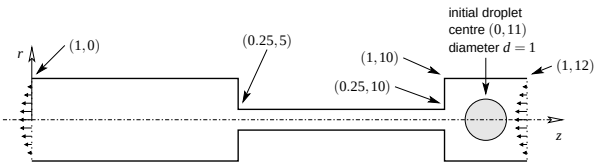

Figure 1: The geometry used in the computational problem. All lengths are normalised by the inlet radius R and cylindrical coordinates (r,z) are used.

Three equations are used to describe motion throughout the disperse (ie, droplet) and continuous phases; a continuity equation, a volume-averaged incompressible Navier–Stokes momentum equation, and an advection equation which describes the evolution of the disperse phase volume fraction ϕ,

$$\nabla \cdot u = 0 \qquad (1)$$

$$\frac{D_u \rho u}{Dt} = -\nabla p + \frac{1}{\mathrm{We}} \kappa \delta(x) n + \frac{1}{\mathrm{Re}} \nabla \cdot \mu [\nabla u + (\nabla u)^{\mathsf{T}}] \qquad (2)$$

$$\frac{D_u \phi}{Dt} = 0 \qquad (3)$$

All three equations are employed in a non-dimensional form. Velocity is scaled by the average inlet velocity, $\bar{v}$, length by the inlet radius R, density by the disperse phase density ρ_{d}^* and viscosity by the disperse phase viscosity μ_{d}^*. The asterix in these equations implies a dimensioned quantity.

The second term on the right of equation (2) is a surface tension induced stress jump which occurs at the disperse-continuous phase interface. In this term κ is the signed local curvature of the interface, $\delta(x)$ is the Dirac delta function, non-zero only on the interface, and n is a unit vector directed normal to the interface and into the disperse phase. As the equations are applied over both phases, the viscosity μ is a function of the local volume fraction, ϕ. The density ρ is not a function of ϕ however as it is assumed to be equal in both phases. Gravitational forces have been neglected as their effect in liquid-liquid micro-sized flows is small.

In this study the behaviour of the droplet as it passes through the contraction is determined by a balance between three types of forces — inertial, viscous and surface tension. Ratios between these forces are given by the Reynolds (Re), Weber (We) and capillary (Ca) numbers, defined by

$$\mathrm{Re} = \frac{\rho_{\mathrm{d}}^* \bar{v} R}{\mu_{\mathrm{d}}^*}, \; \mathrm{We} = \frac{\rho_{\mathrm{d}}^* \bar{v}^2 R}{\sigma} \text{ and } \mathrm{Ca} = \frac{\mathrm{We}}{\mathrm{Re}} = \frac{\bar{v} \mu_{\mathrm{d}}^*}{\sigma},$$

respectively. A simple order of magnitude analysis on momentum equation (2) shows that the strength of surface tension forces relative to both viscous and inertial forces can be mea-

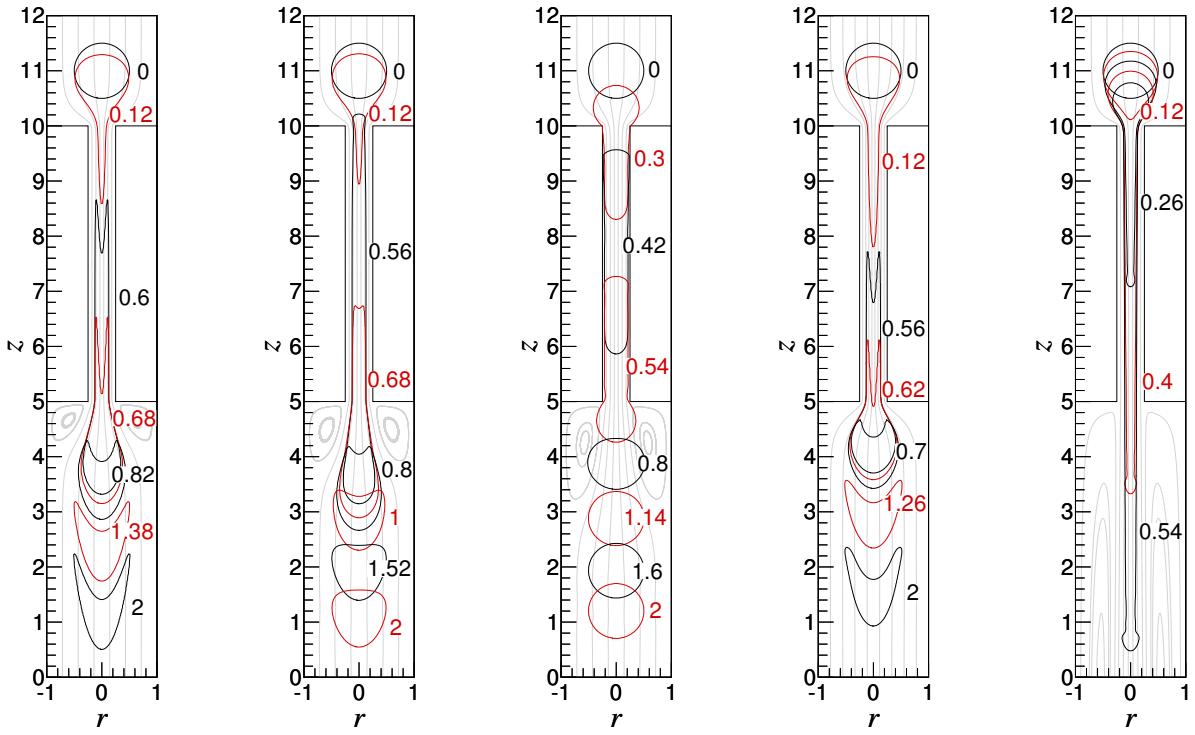

(a) Re = 1.30, We = 100, Ca = 76.8, S = 0.00566

(b) Re = 2.08, We = 1, Ca = 0.481, S = 0.676

(c) Re = 3.33, We = 0.01, Ca = 0.003, S = 76.9

(d) Re = 0.0412, We = 0.1, Ca = 2.42, S = 0.395

(e) Re = 33.3, We = 1, Ca = 0.03, S = 0.971

Figure 2: Images of droplet shapes produced by the Newtonian simulations. Each image was produced by reflecting the two dimensional cylindrical data around the $z = 0$ centreline. In each figure several droplet shapes are shown at the indicated non-dimensional times. The streamlines shown in faint grey were produced by tracing massless particles over a stationary velocity field corresponding to $t = 2$.

sured via another number, termed S. Formally this number is defined as

$$\mathrm{S} = \frac{1}{\mathrm{We} + \mathrm{Ca}} = \frac{\sigma}{\bar{v}\mu_{\mathrm{d}}^{*} + \rho_{\mathrm{d}}^{*}\bar{v}^{2}R}.$$

As a balance between three forces determines droplet behaviour, only two of the above non-dimensional numbers are required to classify a particular flow regime. In the following we use Re and S — Re specifies the ratio of inertial to viscous forces acting in the flow, while S specifies the magnitude of surface tension present, relative to the other forces combined.

Both Newtonian and Non-Newtonian drops are simulated in this study. For the Newtonian cases, we let the continuous phase viscosity equal the disperse phase viscosity so that $\mu = \mu_{\mathrm{d}} = \mu_{\mathrm{c}} = 1$ everywhere. This assumption could be applicable in modelling a light oil droplet entrained in a continuous water phase.

For the Non-Newtonian cases we employ the Carreau model to describe a shear-thinning droplet phase. The Carreau model relates the non-dimensional local disperse phase viscosity μ_{d} to a non-dimensional 'infinite shear rate' viscosity $\mu_{\mathrm{d},\infty}$ via

$$\frac{\mu_{\mathrm{d}} - \mu_{\mathrm{d},\infty}}{1 - \mu_{\mathrm{d},\infty}} = [1 + (\lambda\dot{\gamma})^{2}]^{(n-1)/2}, \qquad (4)$$

where λ is a time constant, n is a 'power-law exponent' and the total shear rate is given by $\dot{\gamma} = \sqrt{\nabla u : [\nabla u + (\nabla u)^{\mathsf{T}}]}$. For the Non-Newtonian cases all viscosities are scaled against the 'zero shear rate' disperse phase viscosity $\mu_{\mathrm{d},0}^{*}$ instead of μ_{d}^{*}. In this study we have chosen $\mu_{\mathrm{d},\infty} = 0$, $\lambda = 1$ and $n = 0.2$. Such values could represent a droplet consisting of a semidilute polystyrene particulate suspension, for example.

Simulation Method

The simulations were performed using a finite volume code due to [7], adapted to model shear-thinning fluids. This code has been successfully used to model the formation and subsequent 'pinch-off' of both Newtonian and Non-Newtonian pendant drops [2] and the deformation of Newtonian droplets through millimeter sized contractions [10]. The Volume of Fluid (VOF) technique is used to track the disperse-continuous phase interface, and surface tension forces are applied using a variation of the Continuum Surface Force (CSF) model. The VOF function is advected using the Youngs scheme. The domain is discretised using a structured, uniform and staggered mesh.

For all of the simulations presented here, a mesh of dimensions 64×768 was used. It was found that using a finer mesh did not significantly alter droplet deformation behaviour. The fluid entering the domain was assumed to have a fully developed Newtonian profile, however tests showed that droplet behaviour within the contraction was quite insensitive to the form of this profile. At the exit the pressure gradient normal to the outlet port was chosen to ensure global mass conservation. All domain walls were non-slip, and non-wetting with respect to the disperse phase liquid. The simulations were performed in series on a Beowulf cluster of Linux boxes with each simulation typically requiring several weeks to complete.

Results: Newtonian Droplets

Figure 2 shows selected droplet shapes at various non-dimensional times for a variety of Re and S numbers. Figure

2(a) shows the results of a simulation conducted with a moderate Re but low S. The low value of S implies that surface tension forces are small here and as a result, surface tension has only a small effect on the deformation of this droplet. A characteristic feature of this simulation is the forked tail that the droplet develops within the contraction. This tail develops because the centreline velocity within the contraction is higher than that near the walls of the contraction. This causes the interface of the droplet near the centreline to move faster through the contraction than the interface located at positions of larger r resulting in the observed 'fork'. As surface tension effects are very weak, the droplet does not return to the form of a sphere before reaching the outlet port.

Figure 2(b) shows a simulation with a similar Re to that shown in figure 2(a), but now with a moderate value for S. The higher surface tension forces act to smooth interface regions of high curvature. As a result, the tail that the previous droplet developed within the contraction is almost absent, and after the droplet leaves the contraction, it returns to a more spherical shape. Figure 2(c) shows a simulation where S has been increased to a high value. Surface tension effects here are so great that significant shape changes only occur when the droplet is constrained by the contraction walls. Thus, within the contraction the droplet forms a long capsule having approximately the same radius of the contraction, while beyond the contraction, it quickly reforms back to its initial spherical state.

Two other moderate S number simulations are shown in figure 2. Figure 2(d) shows a simulation conducted with a S number that lies between that of figure 2(a) and 2(b). As a result the surface tension forces present in this example are greater than those in figure 2(a), but less than those in figure 2(b). Consequently the droplet shapes in figure 2(d) are generally smoother in form than those in figure 2(a), but less spherical than those of figure 2(b). The low Re of figure 2(d) relative to 2(a) appears to have little effect on droplet behaviour, implying that inertial forces in both simulations are almost absent.

Figure 2(e) shows a case with a slightly higher value for S than in figure 2(b), but with a substantially higher Re. The larger inertial effects experienced in this case result in a strong jet of fluid emerging from the contraction, and this jet drives large recirculation zones that extend beyond the computational boundaries. As the recirculation zones extend beyond the computational domain, their behaviour may not be well resolved. However, tests conducted using a variety computational domain sizes have shown that the shape of these recirculation zones does not significantly affect droplet deformation here, most probably because the droplet does not enter these zones during the simulation.

The larger inertial effects present in figure 2(e) mean that the droplet requires a longer time to accelerate at the entrance to the contraction. Once within the contraction however, the droplet forms a fine thread of fluid whose leading tip moves at approximately the contraction centreline velocity, significantly faster than observed in the lower Re cases. As the inertia of this filament is high, its shape remains substantially intact after leaving the contraction.

A characteristic feature of this example is the bulging of the leading tip of the droplet as it moves through the domain. This bulging is the result of surface tension forces which increase the pressure inside the high curvature region at the tip of the thread, in turn pulling this tip back towards the main body of the droplet. The development of this type of bulging has been studied numerically by [5] for the case of low inertia fluids, however a corresponding study for inertial flows is not available.

Results: Non-Newtonian Droplets

Figure 3(a) shows results for a Non-Newtonian droplet. The Re and S numbers used in this simulation, although now based on the zero shear rate disperse phase viscosity, are the same as those used in the example of figure 2(b). At the entrance to the contraction, the fluid experiences both high extensional and shearing strain rates and this causes the viscosity of the droplet phase to decrease. In fact, between the heights of $z = 11$ and $z = 9$ in this example, the viscosity within the droplet decreases by approximately two orders of magnitude. This level of decrease is typical of all of our Non-Newtonian contraction simulations and means that the droplets in these simulations behave in a largely inviscid manner.

An interesting characteristic of shear thinning fluids is that the viscosity generally decreases more than one might expect based on Newtonian strain rate calculations. As the strain rate of a shear thinning fluid increases, its viscosity decreases, leading to smaller viscous stresses. This decrease in viscous stresses generally increases the strain rate, in turn reinforcing the decrease in viscosity. In the droplet shown in figure 3(a) for example, although the strain rate in the continuous phase at the bottom of the computational domain is quite low, the strain rates within the droplet phase are significant as the fluid here is almost inviscid. These high strain rates reinforce the low viscosity, with the result that the viscosity of the leading tip of the droplet remains low for a considerable distance below the lower edge of the contraction. Indeed, the behaviour of this leading tip is quite different to that shown in the Newtonian case of figure 2(b). It is closer to the behaviour displayed in the higher Reynolds number Newtonian case of figure 2(e).

Figure 3(a) also shows that at the indicated time, small disturbances have developed along the interface of the stretched droplet. As both inertial and viscous effects may be important in the continuous phase here, neither the low Reynolds number stability analysis of [9] or the solely inviscid disperse phase analysis of [6] are relevant in predicting the dominant wavelength at which disturbances might grow along this cylinder.

The next three frames, figures 3(b), 3(c) and 3(d), show the movement of a lower Re droplet as it exits the contraction. In this example the strain rates at the contraction entrance are higher than in figure 3(a), so that the viscosity of the droplet phase within the contraction is lower. The two most striking features of this deformation are the large instabilities which grow along the extended droplet, and the unusual 'arrow' shape that forms once the leading tip of the droplet exits the contraction.

As the Reynolds number that characterises this flow is very low, inertial forces within both phases are small relative to viscous forces within the continuous phase, so the behaviour of the droplet is largely determined by the continuous phase viscous forces. This means that the creeping flow stability analysis of [9] is now relevant in predicting the wavelength of maximum capillary wave growth rate on the droplet surface when it is in the contraction. Assuming a constant viscosity ratio of 0.001 within this cylinder, [9]'s analysis suggests that the wavelength of disturbance having the maximum growth rate on the surface of this cylinder would be around 1.0 non-dimensional length units. This appears to be slightly larger than the wavelengths of disturbances displayed in the figure, but of a similar magnitude.

Figures 3(b) through to 3(d) show the development of the leading tip of the droplet as it exits the contraction. As the viscosity of the droplet is low within this region, the deformation of the droplet front is largely determined by the low Reynolds number flow pattern of the surrounding fluid. Thus, as the tip exits the contraction, its front is decelerated and its edges expand radi-

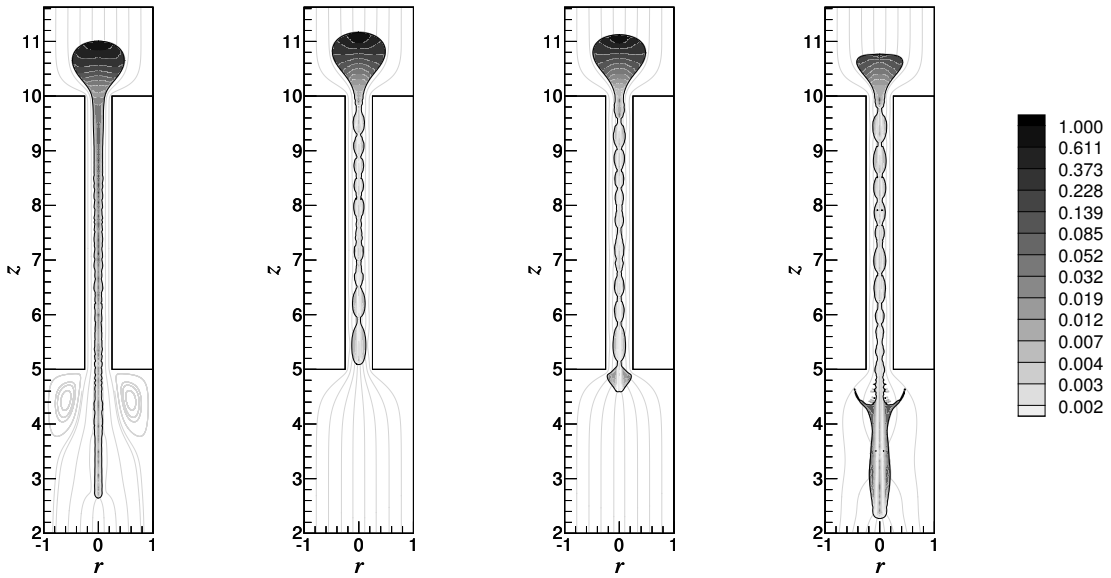

(a) Re = 2.08, We = 1, Ca = 0.481, S = 0.676, $t = 0.28$

(b) Re = 0.0412, We = 0.1, Ca = 2.42, S = 0.395, $t = 0.16$

(c) Re = 0.0412, We = 0.1, Ca = 2.42, S = 0.395, $t = 0.18$

(d) Re = 0.0412, We = 0.1, Ca = 2.42, S = 0.395, $t = 0.34$

Figure 3: Droplet shapes produced by the Non-Newtonian simulations. The streamlines shown in faint grey were produced by tracing massless particles over the instantaneous velocity field of the continuous phase from the indicated time. The shading shows the non-dimensional local viscosity within the drop.

ally, causing it to shorten and 'bulge' (figure 3(c)). After some time elapses however the higher velocity that the droplet experiences along the centreline of the domain advances the centre of the tip further than its slowly advancing radial 'wings'. This results in the unusual 'arrow' type shape seen in figure 3(d). Shapes similar to this have been observed in higher Reynolds number simulations conducted by [10, unreported]. It is interesting to note that even after the tip of the droplet has reached approximately five contraction diameters from the lower edge of the contraction, the viscosity of the droplet is still around three orders of magnitude below the zero shear rate value.

At later times, small amounts of fluid separate from the main droplet just below the contraction exit, as is evident in Figure 3(d). This behaviour is caused by waves along the fluid filament shortening and expanding radially as the droplet exits the contraction and decelerates. While this behaviour appears to be mesh independent, due to the small size of the ejected fluid elements its existence should be treated with caution until experimentally validated.

Conclusions

The deformation of both Newtonian and shear-thinning Non-Newtonian droplets as they pass through an axisymmetric micro-fluidic contraction has been simulated over a range of Re and S. Depending on the balance of inertial, viscous and surface tension forces acting in the fluid, a variety of droplet shapes were simulated including thick 'capsules', thin 'rods' and unstable filaments. Future work will extend the analysis to systems where the viscosity ratio between the two phases is not one, and where droplet breakup is known to occur.

References

[1] Anna, S. L., Bontoux, N. and Stone, H. A., Formation of dispersions using 'flow focusing' in microchannels, *Applied Physics Letters*, **82**, 2002, 364–366.

[2] Davidson, M. R., VOF prediction of drop formation of shear-thinning and yield stress fluids, in *5th International Conference on Multiphase Flow, ICMF'04*, Yokohama, Japan, 2004, paper No. 501.

[3] Eggers, J., Nonlinear dynamics and breakup of free-surface flows, *Reviews of Modern Physics*, **69**, 1997, 865–929.

[4] Funatsu, C. D. H. K., An experimental study of droplet deformation and breakup in pressure-driven flows through converging and uniform channels, *Journal of Rheology*, **22**, 1978, 113–133.

[5] Powers, T. R., Zhang, D., Goldstein, R. E. and Stone, H. A., Propagation of a topological transition: The rayleigh instability, *Physics of Fluids*, **10**, 1998, 1052–1057.

[6] Rayleigh, Lord., On the capillary phenomena of jets, *Proceedings of the Royal Society of London*, **29**, 1879, 71–97.

[7] Rudman, M., A volume-tracking method for incompressible multifluid flows with large density variations, *International Journal for Numerical Methods in Fluids*, **28**, 1998, 357–378.

[8] Stone, H. A., Dynamics of drop deformation and breakup in viscous fluids, *Annual Review of Fluid Mechanics*, **26**, 1994, 65–102.

[9] Tomotika, S., On the instability of a cylindrical thread of a viscous liquid surrounded by another viscous fluid, *Proceedings of the Royal Society of London, Series A*, **150**, 1935, 322–337.

[10] Whyte, D. S., Cooper-White, J., Davidson, M., Lunqvist, A. and Schaerringer, P., Deformation of a droplet passing through a contraction, in *Proceedings of FEDSM2002: 2002 ASME Fluids Engineering Division Summer Meeting*, ASME, Montreal, Quebec, Canada, 2002.